Applied Thermal Engineering 244 (2024) 122733

Contents lists available at ScienceDirect

Applied Thermal Engineering

journal homepage: www.elsevier.com/locate/ate

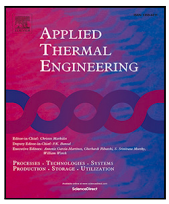

Research Paper

Large Eddy Simulation of Hydrogen/Air MILD combustion in a cyclonic burner

S. Carpenella [a,*], D. Cecere [a], E. Giacomazzi [a], I. Quaranta [a], G. Sorrentino [b], P. Sabia [b], G. Battista Ariemma [b], R. Ragucci [b]

[a] TERIN-PSU-IPSE, ENEA, Rome, Italy
[b] CNR-STEMS, Naples, Italy

ARTICLE INFO

Keywords:
Hydrogen combustion
Large eddy simulation
NO_x formation
MILD

ABSTRACT

In this work Large Eddy Simulation (LES) of a Hydrogen/Air cyclonic burner operating in the MILD combustion regime at 1 atm is performed. The cyclonic flow configuration may represent a proper way to enhance the mixing process in a very short time while allowing for residence times long enough to achieve complete oxidation of diluted and preheated mixtures. Accurate molecular transport properties and a reduced chemical mechanism for hydrogen-air combustion, consisting of 18 transported species and 244 elementary reactions are considered. Results show that at the center of the combustor, where MILD combustion occurs, temperature exhibits a statistically steady trend (a mean of 1450 K) with peak values lower than 1700 K. This implies that the Zeldovich mechanism for thermal NO formation is negligible, so NO levels are low and statistically steady with a maximum peak of 20 ppm. These values are lower than those observed in standard combustion, confirming the ability of MILD to reduce NO_x pollutants also with hydrogen as fuel. Finally, the simulations outcomes are in very good agreement with the experimental results, in particular radiative heat transfer must be taken into account to better capture the preheating of the reactants and consequently fit the experimental temperature profiles in the combustion chamber.

1. Introduction

The design of next-generation burners for heat and power sectors across various industries involves the evaluation of several critical factors, including process efficiency and the achievement of net-zero emissions. Nevertheless, a significant challenge in transitioning to a carbon-neutral future powered by renewable energy sources is related to the exploitation of conversion technologies that can effectively operate with different types of fuel [1]. This is particularly challenging because alternative fuels like hydrogen have significantly different combustion properties compared to fossil fuels [2]. A promising solution to this challenge is the implementation of MILD combustion [3,4], along with related concepts such as Flameless combustion [5] and Colorless Distributed Combustion [6]. These methods involve preheating and diluting the reactants with exhaust gases to create a combustion process with low heat release. In fact, while the heat from the exhaust gases causes an increase in the reactants' temperature, burned gas recirculation dilutes the mixture, reducing the oxygen concentration and maintaining a low temperature in the combustion region. In this combustion process, the reactants feeding temperature is higher than the self-ignition one whereas the maximum allowable temperature increase with respect to inlet temperature during combustion is lower than the ignition temperature [4]. This approach offers enhanced stability, improved fuel flexibility, and reduced emissions, making it a valuable option for sustainable energy systems [7]. Because of the peculiar operative conditions and the presence of locally vitiated reactants conditions, the characteristic times of chemical kinetics and turbulent mixing are comparable and the process is characterized by: distributed reaction zones, relatively uniform temperatures, high radiative heat transfer, no visible flame, noiseless conditions, reduced soot formation, low emissions and fuel flexibility. A particular application of MILD combustion is in processes that employ hydrogen as fuel. In fact, MILD operative conditions allow mitigating the hydrogen characteristics such as its high laminar flame speed, high adiabatic flame temperature, and heating value, high reactivity, which make conventional burners un-suited [8]. The potential for hydrogen to be used as a carbon-free fuel source in MILD combustion offers a unique path forward in the development of greener energy technologies. While numerous literature studies have explored the utilization of hydrogen as a fuel additive to fossil fuels [9,10], there is a scarcity of research when pure

* Corresponding author.
E-mail addresses: simone.carpenella@enea.it (S. Carpenella), giancarlo.sorrentino@stems.cnr.it (G. Sorrentino).

https://doi.org/10.1016/j.applthermaleng.2024.122733
Received 2 November 2023; Received in revised form 12 February 2024; Accepted 13 February 2024
Available online 15 February 2024

hydrogen is used as a fuel in the context of the MILD combustion regime, even though in the latest years several studies have been carried out regarding pure hydrogen combustion, ranging from lab to industrial scales, focused on both experimental and numerical aspects, in atmospheric and pressurized conditions. However, there is a need for additional investigations to address the unresolved issues regarding the fundamental stabilization and reactive region structures in MILD combustion, especially when scale-bridge configurations are considered with strong interactions between fuel/oxidizer and burned gases and with intermediate scales between the lab and the industrial ones. According to the literature, when hydrogen is used as a fuel under MILD combustion, the flame speed tends to increase, such that the reactive regions are more likely to attach close to the burner nozzle, and also cause an increase of the OH concentration in the reaction zone [11].

Moreover, the influence of chemical and mixing timescales on the stabilization of MILD regimes, when hydrogen is used as a fuel, is still an open issue that needs proper investigation. In particular, when methane/hydrogen mixtures are used in MILD Combustion, previous studies showed that reducing the hydrogen in fuel stream leads to increase the reaction zone volume and decrease in flame peak temperature. Such aspect is still unknown when pure hydrogen is used. In this context, the role of the turbulence on the reactive structure and combustion zone weakening is of paramount importance and it needs to be properly investigated under the MILD combustion regime. To address these gaps, the current research leverages the capabilities of Large Eddy Simulation (LES) to examine the impact of hydrogen as a fuel on the structure of MILD reactive regions in conditions of low oxygen concentration, obtained through burned gas recirculation.

Large-eddy simulations, resolving unsteady flow structures, can take into account the turbulence effects with higher accuracies than RANS methods, therefore, improving predictions for turbulent mixing. Due to its high computational cost, most LES studies reported in the literature for MILD Combustion focused their attention on lab-scale systems based on jet flames such as the AJHC [12] or the DJHC burner [13], which can be considered as systems that mimic only locally preheated and diluted reactants conditions. In this specific context, Ihme and See conducted Large Eddy Simulation (LES) of the AJHC [14] utilizing a three-stream flamelet/progress variable formulation to accommodate the hot diluted coflow. When comparing the outcomes with those obtained using a single-mixture fraction formulation, it became evident that the 3FPV model was the only one capable of accurately representing the coflow mixture. Results based on the single-mixture fraction approach resulted in a significant overestimation of both flame temperature and CO mass fraction. The Adelaide Jet in hot coflow was also used as a benchmark case by Li et al. [15] to evaluate the performance of a reactor-based finite-rate model, the partially stirred reactor (PaSR), in comparison to two implicit combustion models, namely, the quasi laminar finite rate (QLFR) and the laminar finite rate (LFR), using various global and detailed kinetic mechanisms. The findings revealed that in a low Damkohler number (Da) process, the adoption of implicit combustion models was well-founded, as they exhibited similar behavior to conventional turbulent combustion models like the partially stirred reactor method. JHC-like flames enable the study of the impact of dilution on the fuel oxidation process without the need to replicate the fluid dynamics responsible for such dilution in realistic scenarios, such as the internal recirculation. Typically, industrial-scale systems employ complex aerodynamics configurations to induce MILD conditions (i.e. reverse flow or swirl/cyclonic motions) within the combustion chamber, where the recirculation of burned products dilutes the incoming reactants.

To realize MILD combustion operating conditions in confined scale-bridging systems [16] that are close to the industrial scale, configurations with high momentum injection of the reactants are adopted: the flue gas recirculation reduces the oxygen concentration in the flame zone, due to a fast mixing between the fuel/oxidizer and the recirculated products stream, and rises the fresh reactants temperature realizing locally distributed ignition conditions throughout the burner volume. An effective method to create the recirculation zone involves the use of a cyclone configuration which allows long residence time inside the combustor by means of a large toroidal recirculation zone, large and multiple reaction zones, high turbulence levels generated from the high shear between oxidant and fuel streams [17]. In this work two Large Eddy Simulation (LES), with and without radiative heat transfer model, of a cyclonic burner operating with pure hydrogen as a fuel in the MILD combustion regime at atmospheric pressure are performed. The paper is organized as follows: Sections 2 and 3 describe the test case definition and the physical models adopted; Section 4 describes the numerical schemes and boundary conditions; Section 5 discusses some key findings of the LES results and their comparisons with available experimental data; conclusions and suggestions for future work follow in Section 6.

2. Test case definition

The test case defined for this study is the Laboratory Unit CYclonic (LUCY) burner [18], a cyclonic flow combustion chamber that ensures the establishment of combustion process under MILD conditions. In this respect, the cyclonic flow entails the intense internal recirculation of combustion products that, in turn, continuously preheat and dilute the inlet reactants, thus attaining MILD conditions. The cyclonic burner is here used as a scale-bridging reactor between the lab scale and the pilot or full industrial ones in order to take into account all the different sub-processes involved in real MILD systems, such as kinetics, turbulence-chemistry interaction, and heat transfer effects between the walls and the reactive region. Indeed, in industrial MILD systems the confinements play a minor role in the flow field evolution and their interaction with the reactive region are less pronounced when compared to the cyclonic burner. Basically, as shown in Fig. 1, the test case consists of a prismatic chamber $20 \times 20 \times 5$ cm^3, operating at atmospheric pressure. The feeding system is composed of by two anti-symmetric couple of inlet jets, placed on the two opposite reactor walls, while the gas exit is located orthogonally with respect to the inlet jets and in the center of chamber bottom face. Such a configuration, along with the chamber internal geometry with chamfered corners in front of the inlet jets (Fig. 1a), induces a cyclonic flow-field. Specifically, the oxidizer and fuel injectors consist of cylindrical ducts with internal diameter of 0.8 cm (oxidizer) and 0.15 cm (fuel). These are located at 2 cm and 4.5 cm from the lateral wall. Furthermore, the oxidizer flow was preheated to the inlet temperature of 550 K, whereas the fuel stream was fed at ambient temperature conditions (300 K). The oxidizer and fuel volumetric flows were adjusted to ensure a nominal equivalence ratio equal to the stoichiometric value ($\Phi = 1$), thus resulting in inlet velocities of 28.9 m/s and 207 m/s, respectively. The combustion process was monitored by means of several N-type thermocouples (nominal diameter 0.15 cm). These were located at the reactor mid-plane (Fig. 1a), to detect the characteristic temperature of the reacting flow, at the burner exit (Fig. 1b), to measure the temperature of the exhaust gases. Furthermore, the temperatures of the reactor internal walls were also monitored, while their average value (equal to 1253 K) was used as boundary conditions for the CFD analysis.

The domain is discretized through 330 internal points along the x-axis, 111 along the y-axis and 250 along the z-axis. Appropriate refinement of the grid is performed in the regions with higher gradients: the minimum grid width is located near the injection zones with $\Delta x = 85\,\mu$m, $\Delta y = 130\,\mu$m and $\Delta z = 350\,\mu$m.

The temperature, and the NO, H_2O and OH mass fractions are sampled with a frequency of 50 kHz both on the yz-plane at $x = 8$ cm and on the xz-plane at $y = 2.5$ cm. Their average values are computed with 1500 samples. In addition, two monitoring points, P1 (in the Air-Jet) and P2 (in the middle of the chamber), are set in the plane of symmetry at x = 0.075 m, z = 0.0 m and x = 0.0 m, z = 0.05 m, respectively, in order to make a spectral analysis. The initial condition

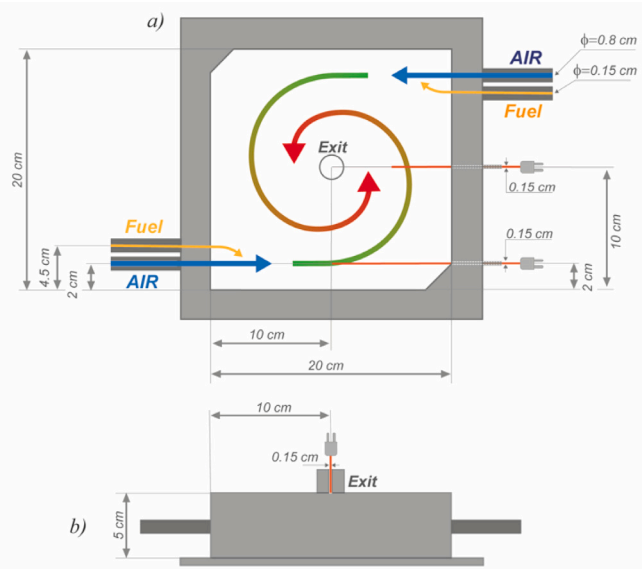

Fig. 1. Sketch of the cyclonic burner.

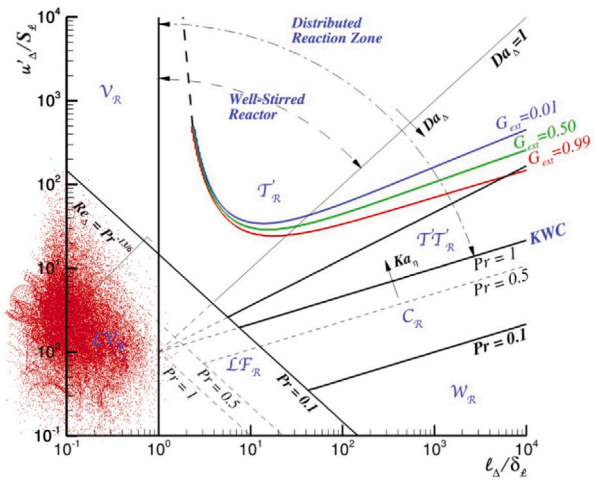

Fig. 2. Example of an instantaneous LTSM combustion diagram [27] (that is not the well known standard combustion diagram).

of the simulation was set to nil velocity flow field and the species settled as combustion products of a 0D MILD chemical reactor simulation. The total simulated time was 0.153 s, while the sampling time was 0.07 s, starting from 0.083 s with a sampling frequency of 200 kHz.

Two LES were conducted with the same conditions: in the first the radiation model M1 is off (LES-noRAD), while in the second is on (LES-RAD).

The simulations were performed on the Linux cluster CRESCO (Computational Center for Complex Systems) at ENEA requiring ~ 6 months on 4000 cores, corresponding to 80 nodes. Each node has 2 CPUs Intel Xeon Platinum 8160 and every CPU has 24 cores with a clock frequency of 2.1 GHz. [19]. The solution was advanced at a constant time step of 6.5 ns, with a CFL (Courant–Friedrichs–Lewy) set to 0.11, in order to ensure the stability of the numerical methods. Such low CFL was necessary to avoid numerical wiggles due to the stiffness of the chemical mechanism.

3. Physical models adopted

In this article the compressible Navier–Stokes equations are solved for a reacting ideal gas flow at atmospheric pressure. The mathematical models adopted are derived for a fluid of N_s chemical species.

A Newtonian fluid is considered and the Stokes' assumption is made. The mass diffusion flux is modeled taking into account its three contributions [20]: the first one due to concentration gradients (Hirschfelder and Curtiss' law for multi-component mixtures) [21], the second due to pressure gradients (the baro-diffusion mechanism) [22], and the third one due to temperature gradients (the thermo-diffusion or Soret effect) [23]. Keeping apart the radiative heat transfer of energy, the heat flux has three contributions too: the first due to temperature gradients (the Fourier diffusion), the second due to mass diffusion fluxes, and the third one is the Dufour effect (reciprocal of the Soret effect). Usually the Dufour effect (the third term) is negligible even when thermo-diffusion is not [23, p. 768] and hence it is neglected in the present work. The mass diffusion coefficient D_i of the ith species into the rest of mixture is modeled according to the Hirschfelder and Curtiss expression [21], where the required binary diffusion coefficient is calculated by means of kinetic theory. The thermo-diffusion coefficient D_i^T is estimated by means of the EGLIB routines [24]. Concerning the radiant transfer of energy, individual species' Planck mean absorption coefficients as a function of temperature, at atmospheric pressure, based on the RADCAL model are adopted [25]. The kinetic scheme here employed is GRI-mech 2.11, excluding Carbon species, as the fuel is pure hydrogen. So, the number of species is reduced from 49 to 18 and the reactions to 244 [26]. The transport equations are solved in the framework of Large Eddy Simulation. The 18 species mass fraction transport equations (including nitrogen compounds and reactions in the combustion mechanism) have been solved, so the NO_x formation is calculated at each time step and coupled with turbulence using the SGS subgrid-scale model. Hence, NO_x formation routes are already included in the combustion mechanisms. Unclosed turbulent combustion subgrid terms of the filtered compressible Navier–Stokes equations are modeled through the dynamic Smagorinsky model and the authors' LTSM (Localized Turbulent Scale Model) [27] turbulent combustion model. The local subgrid velocity fluctuation estimated through the dynamic Smagorinsky model, the local filter size, i.e., the cube root of the cell volume, and the local density and viscosity, determine the local Reynolds number, that is the first input for the LTSM model. It is observed that the Smagorinsky eddy viscosity is very low in most of the computational domain, and particularly in the regions occupied by the hot recirculating gases. This results in very low local subgrid velocity fluctuations, both due to the very fine grid adopted and to the physics of the present configuration: coherently, the rms velocity fluctuations calculated over the sampling time adopted for statistics were as high as ~ 30 m/s very close to the cold reactants injections, but low, < 4 m/s, in the wide volumetric reacting region. In the end, the local Reynolds number is less than one in most of the reacting regions; besides, at some other reacting cells the LTSM model estimates a local spatial scale for combustion larger than the local fluid dynamic scale, i.e., the scale of the cell: hence, in both cases the LTSM model assumes that a perfectly mixed combustion takes place within the whole cell, and the reaction rate coming from the chemical kinetics mechanism is not filtered (the reacting volume fraction of the cell $\gamma^* = 1$). This is evidenced by an instantaneous LTSM combustion diagram [27] (that is not the well known standard combustion diagram) reported in Fig. 2, where blanking of the Heat Release Rate under a value of $2 \cdot 10^6$ W/m^3 was applied to exclude points that do not exhibit important combustion reactions (belonging to inlet jets and hot products recirculation).

The radiant transfer of energy is also taken into account by means of the M_1 diffusive model. It is based on field equations for the radiative energy and the radiative heat flux vector. The limit is that it is valid for non scattering media. The main advantage is that it is independent of the opacity of the media, i.e., it adapts itself and works from thin to thick optical thickness. An averaged form of the M_1 model for turbulent flows exists [28,29] and a simplified formulation of this model was

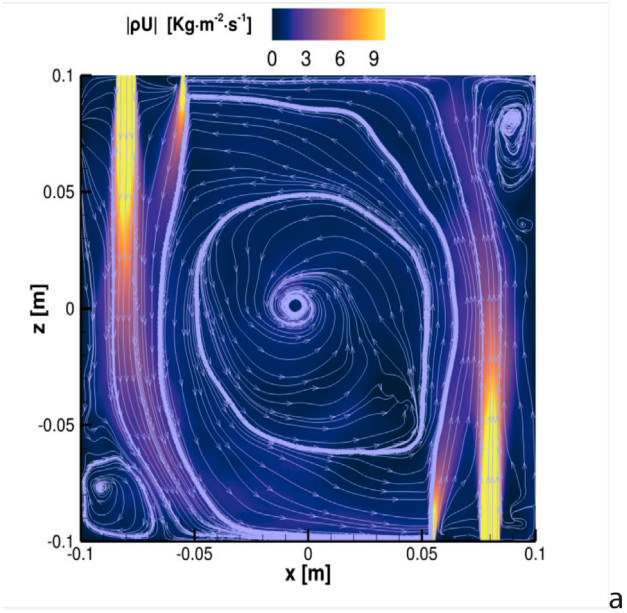

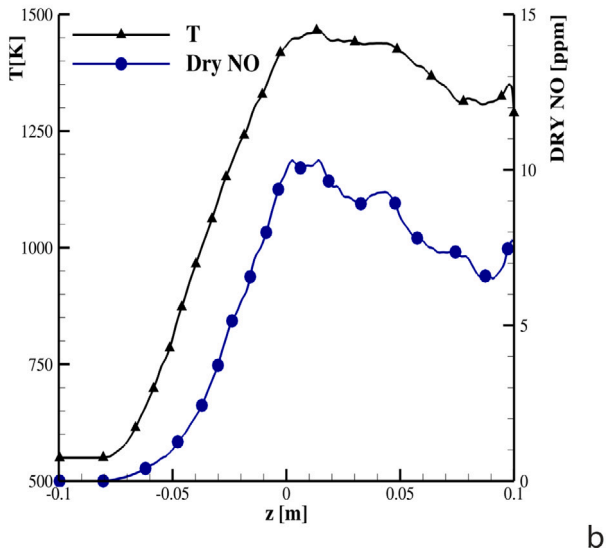

Fig. 3. (a) Average momentum field with streamlines. (b) Predicted average temperature (black delta) and average dry basis NO concentration (blue circles) along the air jet center.

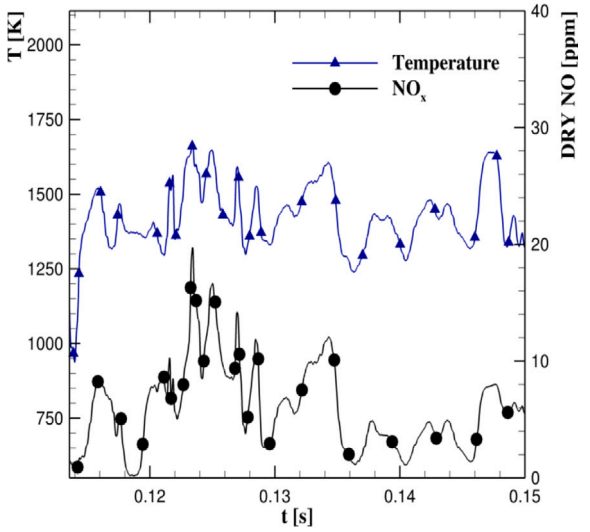

Fig. 4. Temperature and Dry NO concentration time trends at the monitoring point P2.

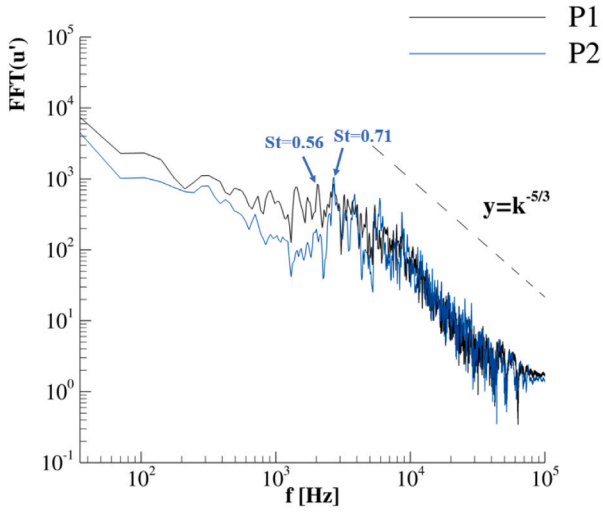

Fig. 5. Velocity Fast Fourier Transform at P1 (Air Jet) and in P2 (Middle) monitoring points. The first peak is at 2030 Hz, the second at 2700 Hz.

finally developed [30]: this is better suited for combustion problems and thus applied in present simulations. In particular, since the original unsteady equations in [28] are very stiff and difficult to solve, a more friendly form is obtained assuming that radiative energy rapidly reaches its equilibrium state, i.e., neglecting the time derivatives. In this way two diffusion equations are obtained for the radiant energy density, E_r $\left[\mathrm{J\,m^{-3}}\right]$, and for its flux vector, $\boldsymbol{F}_r$ $\left[\mathrm{J\,m^{-2}\,s^{-1}}\right]$,

$$\nabla\cdot\left[\frac{1}{\sigma_F}\nabla\cdot\left(\boldsymbol{D}_r E_r\right)\right] = -\left(\sigma_P a T^4 - \sigma_E E_r\right) \tag{1}$$

$$-\nabla\cdot\left[\frac{\boldsymbol{D}_r}{\sigma_E}\nabla\cdot\boldsymbol{F}_r\right] + \sigma_F\boldsymbol{F}_r = -c\nabla\cdot\left[\frac{\sigma_P}{\sigma_E}\boldsymbol{D}_r a T^4\right] , \tag{2}$$

where T is the temperature, $c = 299792458\,\mathrm{m\ s^{-1}}$ is the speed of light, $a = 4\sigma_{SB}/c = 7.565767\cdot 10^{-16}\,\mathrm{J\,m^{-3}\,K^{-4}}$, σ_{SB} being the Stefan–Boltzmann constant, σ_P is the Planck mean absorption coefficient of the mixture (obtained as $\sigma_p = pW\sum_{s=1}^{N} Y_n\sigma_{pn}/W_n$, p is the pressure, W the mixture weight, σ_{pn}, W_n and Y_n the nth species Planck absorption coefficient, the weight and mass fraction respectively), σ_E and σ_F its two effective absorption coefficients (Eq. (23) and 24 in [29]), $\boldsymbol{D}_r$ the non-dimensional Eddington tensor that takes into account the local opacity of the flame. For this flame, the species contributing to the mean absorption coefficient are H_2, O_2, H_2O. For the time being, turbulence-radiation interaction is neglected. The M_1 model (Maximum Entropy approximation) has similarities to the classical diffusion approximations (like P-1), but it is able to better predict directed flux. Consequently, shadowing and long-range transport can be well resolved for a fraction of the cost of methods with exponentially increasing accuracy costs like the method of discrete ordinates and Monte Carlo ray-tracing. Since the M1 method only requires solution of four hyperbolic equations, it may be possible to achieve adequate accuracy for decreased comparative cost. Furthermore, in the P-1 model the media must be optically thick and it may over-predict the radiative fluxes with localized heat sources. In the work of Jensen, six different methods were used to compute the radiative field of a synthetic 2-m, JP-8 pool fire, including Monte Carlo, ray tracing, DOM S4, DOM LC1, DTM, and the M1 moment model [31]. The M1 method was applied

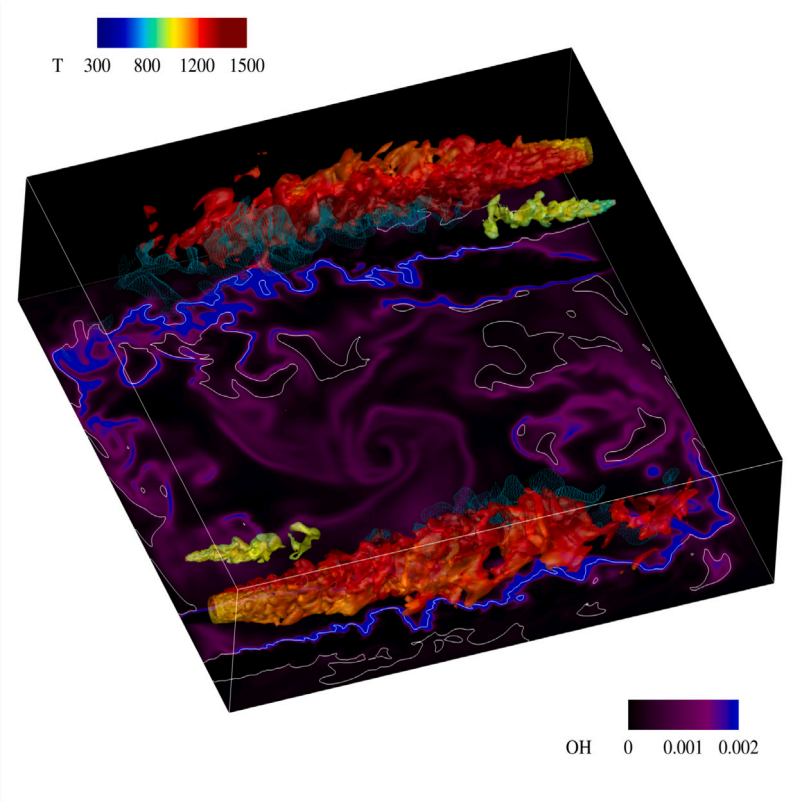

Fig. 6. Instantaneous isosurfaces of oxygen (Y_{O2} = 0.1) and hydrogen (Y_{H2} = 0.1) mass fractions colored with temperature. Green scatter plot of instantaneous Dry NO at 20 ppm. OH instantaneous concentration on the mid-plane (y = 0.025 m) projected to the bottom side of the burner. Isoline of stoichiometric mixture fraction (white line).

for the first time to a combustion problem occurring in a complex three-dimensional geometry. Theoretically, this model has the lowest computational cost among the six, since the directional integration is handled analytically with a model. The M1 model presents results close to the DOM LC11 methods.

4. Numerical schemes and boundary conditions

The numerical simulations are performed by means of the in-house parallel code HeaRT and ENEA's supercomputing facility CRESCO [19]. The HeaRT code solves the compressible Navier–Stokes equations discretized through staggered finite-difference schemes. A second-order accurate centered scheme is adopted for diffusive fluxes; convective terms are modeled through the $AUSM^{+}$-up method [32] coupled with a third/fifth-order accurate $WENO$ interpolation to reduce spurious oscillations (strongly experienced using centered schemes in high-pressure tests); such numerical spatial scheme was extensively tested by the present authors proving its robustness and accuracy [33]. The low-storage third-order accurate Runge–Kutta method of Shu–Osher is used for time integration. The total energy is defined as sum of internal (thermal) and kinetic energy only. The authors found this choice mandatory [34,35] to avoid, or at least reduce, unphysical energy and temperature oscillations, mainly driving to the divergence of calculation. No spurious waves were experienced in previous simulations of premixed flames, when the total energy was defined including the chemical formation contribution. The quasi-steady radiative transfer equations are solved periodically each 10 time steps to update the radiative sink/source term, $\dot{S}_{rad} = -\nabla \cdot \boldsymbol{F}_r \left[\mathrm{W/m^3}\right]$, in the transported total energy equation. They are solved by a fourth order implicit–explicit Peer method [36].

Non-reflecting boundary conditions [37–39] are implemented at open boundaries in their extended form to take into account the effect of variable transport properties [40], local heat release [41].

5. Results

The injection system coupled with the position of the exit and due to its lower pressure allows for the establishment of a toroidal flow field (cyclonic motion) within the chamber. MILD combustion is therefore attained in the combustor due to the strong recirculation process of burned gases toward fresh reactants induced by this toroidal flow field. Fig. 3a shows the average momentum field and the streamlines on a slice at y = 0.025 m. A trapped vortex takes place in the burner as well as two eddies near the corners in front of the jets, due to the presence of the walls. These eddies have a diameter of 2.5 cm, and their presence affects the temperature trends along the air-jet and the mixing process in the combustor. The high hydrogen momentum leads to a sharp change in the flow direction and because of its cross-flow injection, the H_2 jet is curved towards the near air jet; the longer potential core and suction effect of the air jet enhances the hydrogen jet bending.

To analyze in more detail the fluid-dynamic behavior inside the combustor, a frequency analysis was performed using Fast Fourier Transform (FFT) of the fluctuating velocity monitored both at a point in the air jet (P1) and at a point in the center of the burner (P2), as shown in Fig. 5. The trends follow the dissipation of universal turbulent energy, and the FFT amplitude is higher in the air jet compared to that in the center of the combustor. The trapped vortex in the burner has a diameter of approximately 10 cm and an average velocity of 7 m/s, corresponding to a frequency of nearly 70 Hz; such a frequency is not captured by the present numerical simulation, since the sampling time is too short (~ 0.07 s). In addition, two peaks at 2030 Hz and 2700 Hz can be observed: they can be associated with the vortex shedding from the air jet (having a Reynolds Number of 5000), which correspond to a Strouhal Number of 0.56 and 0.71, respectively, coherently with the studies of Becker et al. [42]. The main operational characteristics of the cyclonic combustion burner were investigated through temperature and

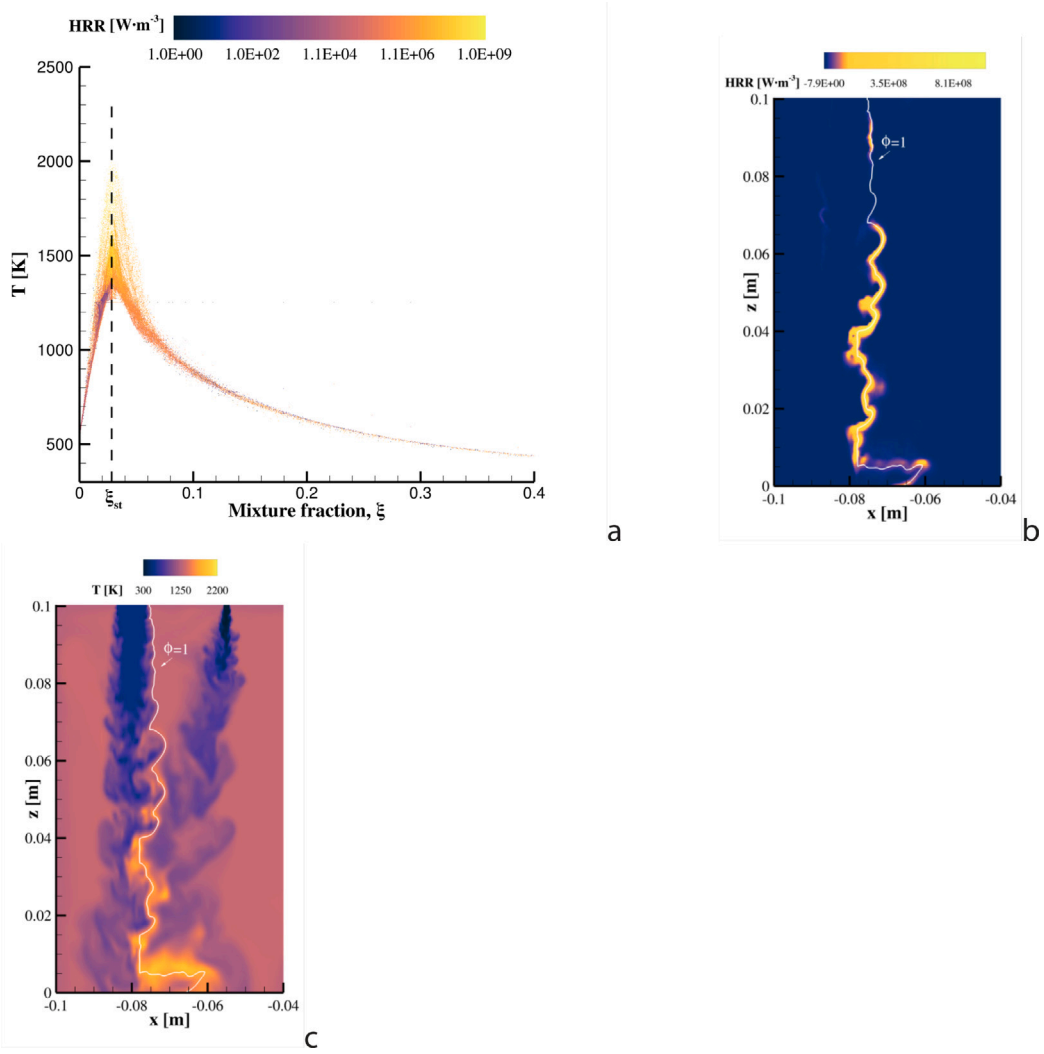

Fig. 7. (a) Scatter plot of instantaneous T profile versus the mixture fraction ξ, colored by Heat Release Rate. (b-c) Instantaneous T and HRR fields with stoichiometric isoline.

exhaust gas emission numerical predictions. MILD Combustion regime was achieved with reduced combustion peak temperatures due to the H_2O recirculation. Fig. 3b reports the predicted average temperature and the average NO concentration profiles along the air jet. The temperature profile is quite uniform from 10 cm downstream of the air injector, with an average value of 1400 K, however it decreases to nearly 1300 K close to the corner eddies, about 2.5 cm from the wall in front of the jets. This temperature condition leads to very low NO emissions. The maximum dry basis NO concentration is lower than 11 ppm and it is located 12 cm downstream of the inlet holes. In addition, the monitoring point P2 at the center of the combustor, where MILD combustion occurs, exhibits a statistically steady temperature trend (a mean of 1450 K) with peak values lower than 1700 K (Fig. 4). This implies that the Zeldovich mechanism for thermal NO formation is negligible, so NO levels are low and statistically steady with a maximum peak of 20 ppm. These values are lower than those observed in standard combustion. The dry basis NO concentration has been evaluated as: $X_{DRY_{NO}} = \frac{X_{NO}}{1-X_{H_2O}}$, where X_{NO} and X_{H_2O} are respectively the NO and H_2O mole fractions.

Fig. 6 shows instantaneous air and hydrogen jet iso-surfaces colored with temperature as well as the OH instantaneous mass fraction on the mid-plane (y = 0.025 m) projected to the bottom side of the burner. The temperature is higher on the side between the air and hydrogen jet, where stoichiometric conditions are reached (see the white line on the bottom plane), radical species are formed contributing to the formation of NO pollutants (see the green scatter of NO [ppm] in Fig. 6) mainly through the thermal mechanism [43] ($T > 1700$ K in this small region).

At the stoichiometric mixture fraction $\xi_{st}(\sim 0.028)$, the highest temperature (nearly 2100 K) is observed, which also corresponds to the highest Heat Release Rate (HRR around 10^9). Anyway the number of points with a temperature greater than 1600 K is very small compared to the total number of points. Fig. 7a shows how the temperature increases with increasing mixture fraction up to ξ_{st}, and then decreases. The highest temperatures and HRR are also located in a small region downstream the two jets where mixing occurs and stoichiometric conditions are reached, as reported in Fig. 7b-c. Fig. 8 reports the average temperature, dry NO, Y_{H2O} and Y_{OH} fields on the y = 0.025 m plane. Maximum concentrations of the radical OH and NO are located at the highest temperatures locations, where diffusive combustion takes place, while, at the center of the chamber, the diluent H_2O has higher concentrations; here MILD conditions are reached and the concentration of the radicals is lower than standard combustion. The homogeneous and distributed temperature, exhibiting average values (~ 1400 K) in the center of the combustor proves that MILD is flameless combustion. Dry NO values smaller than 18 ppm are obtained in the combustor; in particular, they are smaller than 10 ppm in the flameless region. The outlet NO_x emissions in the simulation reached 10 ppm, whereas in the experiment reached 25 ppm. The radiative source term affects the temperature inside the burner: when the term is negative (positive), a sink (source) in the total energy equation is added and a cooling

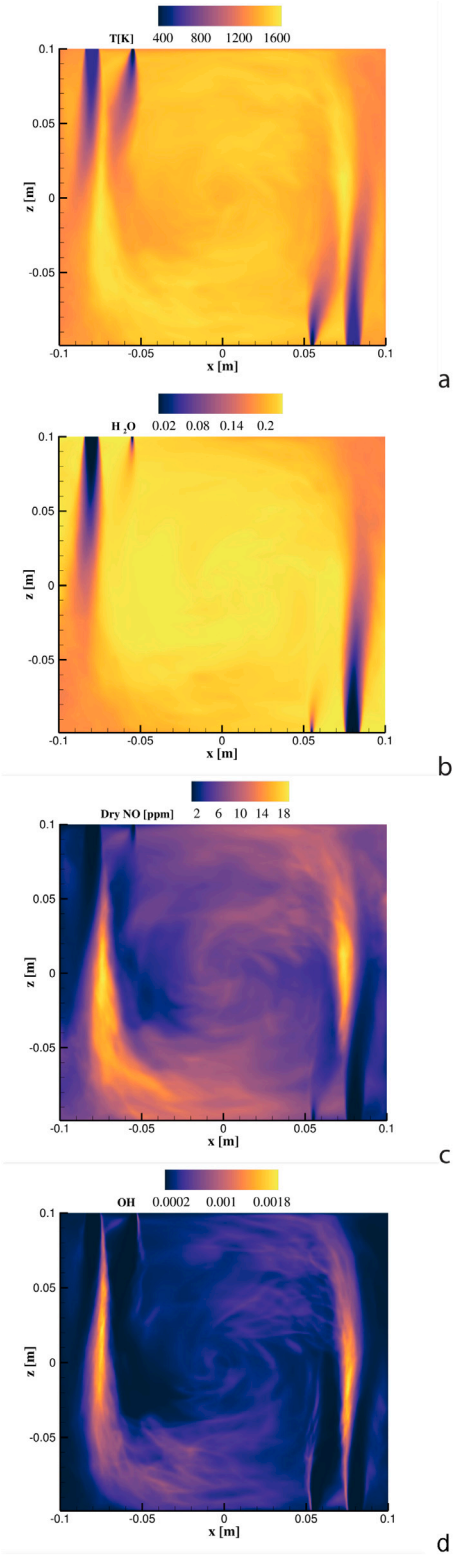

Fig. 8. Average fields of Temperature (a), H_2O mass fraction (b), Dry NO (c) and OH mass fraction (d) at y = 0.025 m.

(heating) effect takes place. In MILD conditions, the radiative source term makes the temperature field more uniform, as shown in Fig. 9: the term is negative at elevated temperatures, while is positive around H_2 and air jets, thanks to H_2O products dilution.

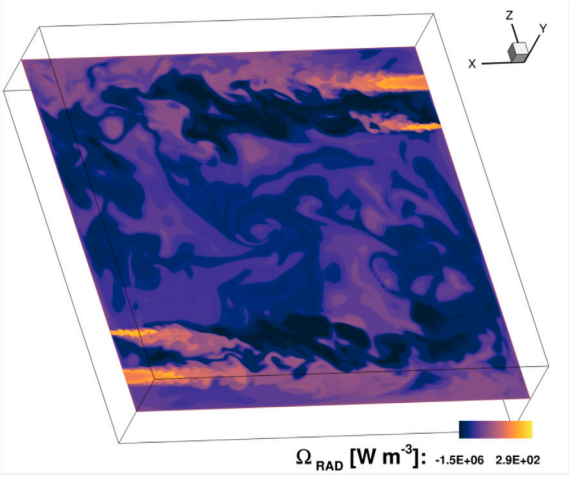

Fig. 9. Snapshot of radiative source term [W m^{-3}] in the total energy equation at y = 0.025 m.

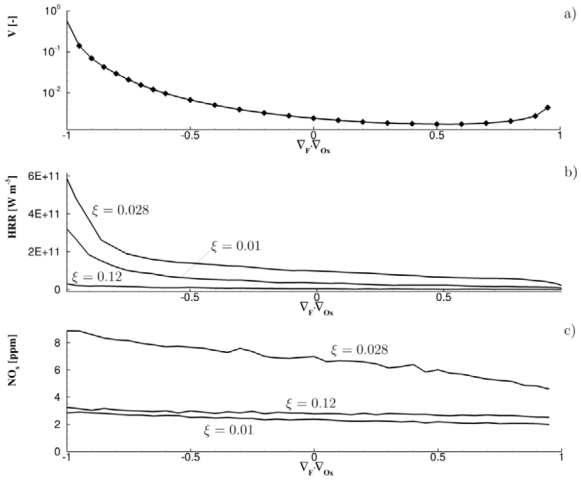

Fig. 10. (a) Volume fraction as a function of the flame index $\nabla Y_F \cdot \nabla Y_{Ox}$, (b) Heat release rate [W m^{-3}] as a function of the flame index and parameterized with the mixture fraction ξ, (c) NO_x concentration [Dry ppm] as a function of the flame index at different values of the mixture fraction ξ.

The turbulent structures deriving from the complex interaction between the fuel jet and the air jet in cross-flow produce intense mixing of reactants. Hence, combustion is likely to happen in both non-premixed and premixed mode, depending on the flow region. The Flame Index helps in identifying such combustion modes even if with an approximation related to the LES simulation where not all turbulence scales are resolved. In particular, the Takeno index is calculated as $FI = \nabla Y_F \cdot \nabla Y_{O_2}/(|\nabla Y_F||\nabla Y_{O_2}|)$, ∇Y_F being the gradient of the fuel species ($Y_F = Y_{H_2}$) [44]. Fig. 10a shows the volume fraction distribution associated to a certain value of the Flame Index, i.e., $V(FI) = \sum_{n=1}^{N_i} V_n(FI)/V_{Tot}$ as a function of the flame index $FI \in [-1, 1]$, N_i being the number of volumes at a fixed value of FI. It can be observed that $FI \in [-1, 1]$: this means that, although the overall flame is non-premixed, reacting structures are associated to both non-premixed ($FI < 0$) and premixed ($FI > 0$) combustion modes even if of two order of magnitude lower. Fig. 10b reports the mean heat release rate distribution as a function of the Flame Index and mixture fraction ξ. The maximum heat release is found in regions near the stoichiometric mixture fraction ($\xi \sim 0.028$) and for positive values of the Flame Index, associated to premixed combustion. The heat release from the diffusion flame is located immediately downstream between the fuel and air jets

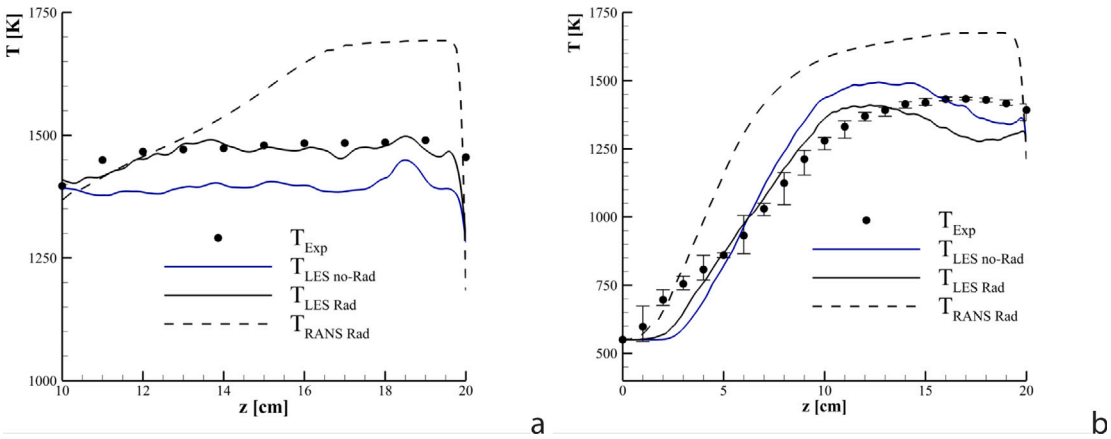

Fig. 11. (a) LES (line) vs. Experimental (dot) vs. RANS (dashed line) average temperature profile along z-axis in the middle plane (xz) at x = 0.0 m. (b) LES (line) vs. Experimental (dot) vs. RANS (dashed line) average temperature profile along z-axis in the middle plane along the air-jet center (x = − 0.08 m).

and here the heat release reachs its maximum value corresponding to the stechiometric mixture fraction and decreasing as the mixture fraction increases. Fig. 10c shows the mean NO pollutant concentration in dry ppm (dppm) as a function of the Flame Index and mixture fraction ξ. As in the case of heat release, the pollutants are mostly formed in the near stoichiometric regions, with the maximum values reached in diffusion flame zones ($FI < 0$). However, by increasing the mixture fraction, the NO concentration decreases much less than the heat release and values around 3 ppm are found in rich flame regions.

In order to validate the obtained results, a comparison has been made with experimental data and RANS results previously obtained. RANS simulations were performed by ANSYS Fluent, employing the Reynolds Stress Model (RSM) [45] and assuming incompressible and ideal gas conditions. On the other hand, the Enhanced Wall Treatment (EWT) [45] was adopted as near-wall modeling method. The radiative transport was handled by the Discrete Ordinate (DO) method with the weighted-sum-of-grey-gas (WSGG) approach [46]. The interaction between chemical kinetic and turbulent mixing was modeled by the Partially Stirred Reactor (PaSR) model [47], with the mixing timescale equal to a fraction of the integral timescale ($C_{mix} = 0.5$) [48]. Fig. 11 shows that LES can capture the experimental detected behavior properly when compared to RANS ones. This is mainly due to the accurate representation of turbulent mixing and molecular transport effects obtained by LES simulations and that are not taken into account when RANS modeling environment is used. In particular, the effects related to the mixing of the oxidant jet with the recirculated products are well reproduced by LES.

Furthermore, the effect of the M1 radiation model in the Large Eddy Simulation was evaluated. Fig. 11 shows that LES temperature results with radiation model are in more agreement with experimental measurements than without M1. In general, the major effects of the radiating heat transfer is to preheat the absorbing lower temperature regions (the inlet jets in this case), and to lower the high temperature of stoichiometric reacting regions. Although this general effects, temperature of reacting zones can increase due to the higher inlet temperature of the reactants. The simulation does not well capture the temperature profile close to the injection holes: this could be mainly attributed to the presence of thermocouples (1.5 mm thick vs 8 mm of the air initial jet diameter) that perturb the fluid dynamics of the air jet and increases mixing with hot recirculating hot products; moreover, the inlet turbulent boundary conditions at the air holes were not experimentally characterized. The temperature trend near the wall downstream of the air jet does not approximate very well the experimental results due to the presence of a stationary vortex, with an average diameter of 2.5 cm. Such a vortex is due to the different local geometry of the LES simulation, where the 45° inclined plane in front of the jets was replaced by a 90° corner (the grid is cartesian). The main advantage of using the radiative model is clearly visible in Fig. 11b: the error decreases from a maximum of 9% (LES-noRAD) to a maximum of 1.5% (LES-RAD).

6. Conclusions

In the present work, the main operational characteristics of a hydrogen/air cyclonic burner operating in the MILD combustion regime at atmospheric pressure were investigated by means of Large Eddy Simulation. The M1 macroscopic radiation model was adopted to evaluate the effects of the radiating transfer of energy: it contributes to increase inlet jet temperatures and uniform temperature field inside the burner, with an average value around 1450 K. The highest temperatures and Heat Reaction Rate, located in small pockets of the shear layer, were found at the stoichiometric equivalence ratio regions. Also, the maximum dry NO concentration was found where the highest temperatures are exhibited, reaching a value of nearly 20 ppm, confirming that MILD combustion is a promising technique to reduce pollutant emissions. Finally, the numerical results exhibit a remarkable alignment with the experimental data. Notably, the incorporation of radiative heat transfer is crucial for more accurate predictions.

Future works could investigate MILD combustion behavior at higher pressures for micro gas-turbine applications, and also examine the use of pure-ammonia and hydrogen-ammonia blends as potential fuels.

CRediT authorship contribution statement

S. Carpenella: Conceptualization, Data curation, Supervision, Writing – original draft, Writing – review & editing, Investigation. **D. Cecere:** Conceptualization, Data curation, Software, Writing – review & editing, Investigation. **E. Giacomazzi:** Conceptualization, Supervision, Writing – original draft, Writing – review & editing. **I. Quaranta:** Data curation. **G. Sorrentino:** Conceptualization, Data curation, Investigation, Writing – original draft, Writing – review & editing. **P. Sabia:** Conceptualization, Data curation, Formal analysis, Methodology. **G. Battista Ariemma:** Conceptualization, Data curation, Investigation, Writing – original draft, Writing – review & editing. **R. Ragucci:** Conceptualization, Data curation, Formal analysis, Methodology.

Declaration of competing interest

The authors declare that they have no known competing financial interests or personal relationships that could have appeared to influence the work reported in this paper.

Data availability

If someone asks for LES data they will be available, but the code will not be accessible.

Acknowledgments

The computing resources and the related technical support used for this work have been provided by CRESCO/ENEAGRID High Performance Computing infrastructure and its staff [19]. CRESCO/ENEAGRID High Performance Computing infrastructure is funded by ENEA, Germany, the Italian National Agency for New Technologies, Energy and Sustainable Economic Development and by Italian and European research programmes (see http://www.cresco.enea.it/english (accessed on 31 October 2023)).

References

[1] G. Sorrentino, P. Sabia, P. Bozza, R. Ragucci, M. de Joannon, Impact of external operating parameters on the performance of a cyclonic burner with high level of internal recirculation under MILD combustion conditions, Energy 137 (2017) 1167–1174.
[2] E. Giacomazzi, G. Troiani, A. Di Nardo, G. Calchetti, D. Cecere, G. Messina, S. Carpenella, Hydrogen combustion: Features and barriers to its exploitation in the energy transition, Energies 16 (20) (2023) 7174.
[3] D. Cecere, E. Giacomazzi, F.R. Picchia, N. Arcidiacono, LES of $H2 \setminus Air$ MILD combustion, in: Proceedings of the 31st Meeting of the Italian Section of the Combustion Institute, 2008.
[4] A. Cavaliere, M. de Joannon, Mild combustion, Prog. Energy Combust. Sci. 30 (2004) 329–366.
[5] M. Ayoub, C. Rottier, S. Carpentier, C. Villermaux, A.M. Boukhalfa, D. Honoré, An experimental study of mild flameless combustion of methane/hydrogen mixtures, Int. J. Hydrogen Energy 37 (8) (2012) 6912–6921.
[6] V.K. Arghode, A.K. Gupta, K.M. Bryden, High intensity colorless distributed combustion for ultra low emissions and enhanced performance, Appl. Energy 92 (2012) 822–830.
[7] P. Sabia, G. Sorrentino, G.B. Ariemma, M.V. Manna, R. Ragucci, M. de Joannon, MILD combustion and biofuels: A minireview, Energy Fuels 35 (24) (2021) 19901–19919.
[8] C. Galletti, A. Parente, M. Derudi, R. Rota, L. Tognotti, Numerical and experimental analysis of NO emissions from a lab-scale burner fed with hydrogen-enriched fuels and operating in MILD combustion, Appl. Therm. Eng. 34 (2009) 8339–8351.
[9] Y. Afarin, S. Tabejamaat, Effect of hydrogen on H2/CH4 flame structure of mild combustion using the LES method, Int. J. Hydrogen Energy 38 (8) (2013) 3447–3458.
[10] A. Mardani, H.K.M. Mahalegi, Hydrogen enrichment of methane and syngas for MILD combustion, Int. J. Hydrogen Energy 44 (18) (2019) 9423–9437.
[11] A. Parente, C. Galletti, L. Tognotti, Effect of the combustion model and kinetic mechanism on the MILD combustion in an industrial burner fed with hydrogen enriched fuels, Int. J. Hydrogen Energy 33 (2008) 7553–7564.
[12] B.B. Dally, A.N. Karpetis, R.S. Barlow, Structure of turbulent non-premixed jet flames in a diluted hot coflow, Proc. Combust. Inst. 29 (1) (2002) 1147–1154.
[13] E. Oldenhof, M.J. Tummers, E.H. van Veen, D.J.E.M. Roekaerts, Ignition kernel formation and lift-off behaviour of jet-in-hot-coflow flames, Combust. Flame 157 (6) (2010) 1167–1178.
[14] M. Ihme, Y.C. See, LES flamelet modeling of a three-stream MILD combustor: analysis of flame sensitivity to scalar inflow conditions, Proc. Combust. Inst. 33 (1) (2011) 1309–1317.
[15] Z. Li, A. Cuoci, A. Parente, Large eddy simulation of MILD combustion using finite rate chemistry: effect of combustion sub-grid closure, Proc. Combust. Inst. 37 (2019) 4519–4529.
[16] L. Giuntini, L. Frascino, G.B. Ariemma, C. Galletti, G. Sorrentino, R. Ragucci, Performance assessment of modeling approaches for moderate or intense low-oxygen dilution combustion in a scale-bridging burner, Energy Fuels 37 (13) (2023) 9500–9513.
[17] G.B. Ariemma, G. Sorrentino, P. Sabia, R. Ragucci, M. de Joannon, MILD combustion of methanol, ethanol and 1-butanol binary blends with ammonia, Proc. Combust. Inst. 39 (4) (2023) 4509–4517.
[18] G.B. Ariemma, et al., Alcohols as energy carriers in MILD combustion, Energy Fuels 35 (9) (2021) 7253–7264.
[19] G. Ponti, et al., A the role of medium size facilities in the HPC ecosystem: the case of the new CRESCO4 cluster integrated in the ENEAGRID infrastructure, in: Proceedings of the 2014 International Conference on High Performance Computing and Simulation, HPCS, 2014, pp. 1030–1033.
[20] E. Giacomazzi, F.R. Picchia, N. Arcidiacono, A review on chemical diffusion, criticism and limits of simplified methods for diffusion coefficients calculation, Combust. Theory Model. 12 (2008) 135–158.
[21] J.O. Hirschfelder, C.F. Curtiss, R.B. Bird, E.L. Spotz, The Molecular Theory of Gases and Liquids, John Wiley & Sons, 1954.
[22] N. Babkovskaia, N.E.L. Haugen, A. Brandeburg, A high-order public domain code for direct numerical simulations of turbulent combustion, J. Comput. Phys. 230 (2011) 1–12.
[23] R.B. Bird, W.E. Stewart, E.N. Lightfoot, Transport Phenomena, second ed., John Wiley and Sons, 2002.
[24] A. Ern, V. Giovangigli, EGlib: A general-purpose fortran library for multicomponent transport property evaluation, Manual EGlib version 3 (4) (2004).
[25] W.L. Grosshandler, RADCAL: A Narrow-Band Model for Radiation Calculations in a Combustion Environment, NIST Technical Note 1402, 2011, pp. 1–12.
[26] C.T. Bowman, R.K. Hanson, D.F. Davidson, W.C. Gardiner, V. Lissianski, G.P. Smith, D.M. Golden, M. Frenklach, M. Goldenberg, http://www.me.berkeley.edu/gri_mech/.
[27] E. Giacomazzi, D. Cecere. A., Combustion regime-based model for large eddy simulation, Energies 14 (16) (2021) 4934.
[28] J.-F. Ripoll, B. Dubroca, G. Duffa, Modelling radiative mean absorption coefficients, Combust. Theory Model. 5 (2001) 261–275.
[29] J.-F. Ripoll, An averaged formulation of the M1 radiation model with presumed probability density functions for turbulent flows, J. Quant. Spectrosc. Radiat. Transfer 83 (2004) 493–517.
[30] J.-F. Ripoll, H. Pitsch, Modelling turbulence-radiation interactions for large sooting turbulent flames, Annu. Res. Briefs (2002) 41–52.
[31] Kirk A. Jensen, Jean-François Ripoll, Alan A. Wray, David Joseph, Mouna El Hafi, On various modeling approaches to radiative heat transfer in pool fires, Combust. Flame 148 (4) (2007) 263–279.
[32] M.S. Liou, A sequel to AUSM, Part II: AuSM$^+$-up for all speeds, J. Comput. Phys. 214 (2006) 137–170.
[33] E. Giacomazzi, D. Cecere, N.M.S. Arcidiacono, G. Rossi, F.R. Picchia, LES Code Development and Validation, CIRA - Italian Aerospace Research Center, 2017.
[34] E. Giacomazzi, D. Cecere, N.M.S. Arcidiacono, F.R. Picchia, Approaching the numerical simulation of trans- and super- critical flows, in: 8th European Combustion Meeting, 2017.
[35] E. Giacomazzi, D. Cecere, N.M.S. Arcidiacono, F.R. Picchia, G. Rossi, L. Cutrone, A. Mastellone, Numerical simulations of high-pressure mixing and combustion, in: AIAA Propulsion and Energy Forum, 2017.
[36] M. Schneider, J. Lang, R. Weiner, Super-convergent implicit-explicit peer methods with variable step sizes, J. Comput. Appl. Math. 387 (2021).
[37] D.H. Rudy, J.C. Strikwerda, A boundary conditions for subsonic compressible Navier–Stokes calculations, Comput. & Fluids 9 (1981) 327–338.
[38] K.W. Thompson, A boundary conditions for subsonic compressible Navier–Stokes calculations, J. Comput. Phys. 89 (1990) 439–461.
[39] T.J. Poinsot, S.K. Lele, Boundary conditions for direct simulations of compressible viscous flows, J. Comput. Phys. 101 (1992) 104–129.
[40] M. Baum, T. Poinsot, D. Thévenin, Accurate boundary conditions for multicomponent reactive flows, J. Comput. Phys. 116 (1995) 247–261.
[41] J.C. Sutherland, C.A. Kennedy, Improved boundary conditions for viscous, reacting, compressible flows, J. Comput. Phys. 191 (2003) 502–524.
[42] H.A. Becker, T.A. Massaro, Vortex evolution in a round jet, J. Fluid Mech. 31 (part 3) (1968) 435–448.
[43] D. Cecere, E. Giacomazzi, A. Di Nardo, G. Calchetti, Gas turbine combustion technologies for hydrogen blends, Energies 16 (19) (2023) 6829.
[44] T. Zirwes, F. Zhang, P. Habisreuther, M. Hansinger, H. Bockhorn, M. Pfitzner, D. Trimis, Identification of flame regimes in partially premixed combustion from a Quasi-DNS dataset, Flow Turbul. Combust. 106 (2021) 373–404.
[45] ANSYS, Fluent ANSYS, ANSYS Fluent Theory Guide 19 (1) (2019).
[46] W.A. Fiveland, Discrete-ordinates solutions of the radiative transport equation for 410 rectangular enclosures, J. Heat Transf. 106 (1984) 699–706.
[47] J. Chomiak, Combustion A study in theory, fact and application, 1990.
[48] R. Amaduzzi, G. Ceriello, M. Ferrarotti, G. Sorrentino, A. Parente, Evaluation of modeling approaches for MILD combustion systems with internal recirculation, Front. Mech. Eng. 6 (2020) 516156.